Published in *International Journal of Electrical Power & Energy Systems*, vol. 142, part A, which should be cited to refer to this work.
DOI: 10.1016/j.ijepes.2022.108186

On the Reconstruction of the Attenuation Function of a Return-Stroke Current from the Fourier Transform of Finite-Duration Measurements

Riccardo Aramini[a], Massimo Brignone[a], Daniele Mestriner[a], Matteo Pastorino[a], Renato Procopio[a], Farhad Rachidi[b], Andrea Randazzo[a], Marcos Rubinstein[c]

[a] *Department of Naval, Electrical, and ICT Engineering (DITEN), University of Genoa, Via Opera Pia 11a, Genova, I-16145, Italy*
[b] *Electromagnetic Compatibility (EMC) Laboratory, Swiss Federal Institute of Technology of Lausanne (EPFL), Lausanne, 1015, Switzerland*
[c] *Institute for Information and Communication Technologies, Haute École d'Ingégnerie et de Gestion du Canton de Vaud (HEIG-VD), Yverdone-les-Bains, 1401, Switzerland*

Abstract

A correct representation of the lightning current is crucial when the electromagnetic field radiated to a point of interest has to be computed. Based on the engineering models of Transmission Line type, such representation involves the knowledge of the return-stroke speed, the channel-base current, the channel height and the attenuation function. Whereas the first three quantities can be measured in different ways, no measurement technique can directly provide reliable information on the attenuation function. In the past decades, researchers have applied various strategies to address this problem. These strategies are all based on a common feature, i.e., the unknown function is postulated a priori and then validated through the comparison of the computed electromagnetic fields at one or more observation points with the corresponding measured waveforms. In this paper, we propose an alternative approach for the identification of the attenuation function: starting from appropriate measurements of the return-stroke speed, the channel-base current, the channel height and the radiated electromagnetic field, we first formulate an algebraic inverse and ill-posed problem, obtained from the discretization of integral equations relating the source to the radiated field in the frequency domain, and then we solve it by means of a Tikhonov regularization technique. The proposed framework is preceded by a detailed theoretical analysis,

with special emphasis on the description and filtering of measurement noise and on the minimum duration of the measurement time-windows ensuring reliable results.

Keywords: lightning, electromagnetic fields, inverse problems
PACS: 0000, 1111
2000 MSC: 0000, 1111

---

1. Introduction

Lightning is one of the most critical phenomena affecting the reliability of electrical systems [1, 2]. The need for a correct computation of the electromagnetic (EM) fields illuminating an electrical infrastructure is crucial and has been deeply analyzed during the past decades. The EM fields are usually computed starting from the postulated knowledge of the current spatial-temporal distribution along the lightning channel; in this framework, five different modeling approaches have been developed:

1. gas dynamic or physical models [3, 4, 5]: they require three hydrodynamic equations (representing the conservation of mass, momentum and energy) to be solved and coupled to two state equations admitting, as an input parameter, a postulated and time-dependent channel current;
2. electromagnetic or antenna-theory models (e.g., [6, 7]), whereby the lightning channel is regarded as a lossy thin-wire antenna;
3. distributed circuit models (e.g., [8]), which represent an approximation of the electromagnetic models and utilize the telegrapher equations to describe the lightning channel;
4. waveguide models (e.g., [9, 10]): they model the lightning channel as a waveguide with finite conductivity and represent the return stroke as a current pulse traveling in it;
5. engineering models, which can in turn be subdivided into three categories [11], i.e., Current Propagation (or Transmission Line type) models (e.g., [12, 13, 14, 15]), Current Generation (or Travelling Current Source type) models [16, 17, 18, 19, 20] and Current Dissipation models (e.g., [21, 22]).

When dealing with the interactions of lightning with electrical infrastructure, engineering models are most frequently adopted, owing to their low

computational cost in the evaluation of the EM fields. Moreover, they satisfactorily represent the EM fields from tens of meters up to hundreds of kilometers from the lightning stroke [16]. Under the assumption of a vertical lightning channel, this approach provides an equation relating the channel current $I(z', t)$ at any time t and height z' to the channel-base current: depending on the particular application, the time-domain waveform of such current at $z' = 0$ is either measured or modeled (with a small number of adjustable parameters) on the basis of data sets collected by measurement campaigns in different parts of the world.

Among the engineering models, the most common choice is represented by the Transmission Line (TL) type models, characterized by the general equation

$$I(z', t) = u\left(t - \frac{|z'|}{v_f}\right) P(z')\, I\left(0, t - \frac{|z'|}{v}\right), \tag{1}$$

where u is the unit step function, v_f is the return-stroke speed, v is the current-wave propagation speed (usually $v = v_f$), $P(z')$ is the attenuation function and $I(0, t)$ is the channel-base current. If the trivial case $P(z') \equiv 1$ is a priori excluded, they are referred to as modified TL (MTL) models. Note that TL-type models assume that no distortion occurs along the channel. According to several measurements all around the world, the return-stroke speed turns out to vary from one third to one half of the light speed [23]. Moreover, thanks to the use of the well-known Rogowski coil (or other devices, such as shunts), instrumented towers (e.g., [24, 25, 26, 27, 28]) allow measuring the channel-base current, thus leading to a set of lightning channel-base current parameters, which are commonly adopted in various standards [1]. Experimental results in this field have inspired the definition of different kinds of functions to represent the channel-base current [29, 30, 31, 32, 33, 34].

On the other hand, the attenuation of the current along the stroke channel is a critical point in the lightning research, since information on this property is difficult to obtain by direct measurements. To address such issue, the most frequently adopted models are based on the following strategy: first, a parameterized formula is postulated a priori for $P(z')$; then, the parameters are adjusted in order to achieve the best fit with the measured EM fields. This approach results in the well-known MTLL [13], MTLE [14], MTLTCOS, MTLTSIN, MTLT and MTLT2 models [15].

A second and more complex approach consists in regarding the "current-field equations", i.e., the integral equations relating the channel current to

the radiated EM fields, as an inverse problem, whose unknown is the attenuation function, whereas the input data are appropriate measurements of the EM fields, as well as of the return-stroke speed, the channel height and the channel-base current. Through discretization, an algebraic and linear inverse problem is thus obtained, which can be solved by using suitable regularization techniques. In principle, this problem can be formulated either in the time domain (see, e.g., [35]) or in the frequency domain, but the latter case seems to be more adequate for many purposes: see, e.g., [36, 37, 38, 39, 40].

In spite of the coherent theoretical framework and some promising results, there are some significant issues that still need to be properly tackled if the prospective application to real-data inversion is to be taken into account. First, the standard Fourier Transform (FT) requires, in principle, measurement times of infinite duration, which is obviously impossible in any realistic application; on the other hand, if their finiteness is explicitly considered, as recently shown in [41], the integral equations for the vertical and radial components of the electric field need to be modified with respect to the standard formulation (to be found in [42]) and become more complex. Second, one of the main advantages of working in the frequency domain is the possibility of filtering out, at least to some extent, the measurement noise by means of a procedure analogous to low-pass filtering; however, this possibility does not seem to have been fully exploited so far, since simulated noise has been directly added to the data in the frequency domain (see, in particular, [37, 38]) instead of obtaining it as the FT of a properly modeled noise in the time domain. A possible exception to this tendency can perhaps be found in some short hints given by [39]; however, in [39] noise was only added to the electric field and not to the channel-base current.

The main goal of this paper is to fill these two gaps by proposing a framework where both the finite duration of time-domain measurements and a realistic modeling of measurement noise in the time domain (with its subsequent low-pass filtering) are systematically considered in the formulation of the inverse problem of interest. More precisely, the various sections forming this paper can be outlined as follows.

In Section 2, we first introduce the geometry of the problem and summarize the results obtained in [41], which rely on the assumption that the measurement times are sufficiently long (but finite); in particular, we recall the current-field equations, both in the time domain and in the frequency domain. Then, by applying such results to the case of an MTL model for the return-stroke current, we deduce the integral equations representing the

theoretical formulation of the inverse problem to be addressed. In Section 3, the previous equations are discretized in the frequency domain, thus recasting the inverse problem as a linear algebraic system. Next, we describe in detail both the numerical computation of noiseless data and the simulation of the measurement noise affecting the EM fields and the channel-base current; also some source of model noise (i.e., of discrepancy between the actual implementation and the true values of the parameters or the assumptions of the model) is briefly considered. Finally, we outline the inversion and regularization procedures applied to solve the ill-posed inverse problem, i.e., Tikhonov regularization coupled with the L-curve method for the choice of the regularization parameter. Section 4 is devoted to the presentation and discussion of the obtained results, i.e., the reconstructions of the attenuation function $P(z')$ in several different conditions, by varying the models for $P(z')$, the choices of the measured fields, the accuracy of the knowledge of the return-stroke speed and the duration of the measurement times. Lastly, our conclusions are presented in Section 5.

2. Theoretical formulation of the inverse problem in the case of finite-duration time-windows

2.1. Preliminary review of known results

With reference to Fig. 1, we consider a lightning return stroke whose channel is vertical and rectilinear, has a finite length H and lies on the z-axis of a Cartesian orthogonal coordinate system with the origin O placed at the base of the channel. Let $z' \in [0, H]$ be the height of any point Q_1 on the return-stroke channel and let $(r, z) \in (0, +\infty) \times \mathbb{R}$ be the pair formed by the radial coordinate and the height of the measurement point Q_2, where the electric and/or magnetic fields radiated by the lightning return-stroke are observed; then, the distance between Q_1 and Q_2 is

$$R(z') = \sqrt{r^2 + (z - z')^2} \tag{2}$$

and, in particular, for $Q_1 \equiv O$ (i.e., $z' = 0$), $R(0) = \sqrt{r^2 + z^2}$.

We require that no secondary source of radiation be present other than the ground: the latter is modeled as an infinite, horizontal and perfect electric conducting (PEC) plane, which enables applying the method of images; accordingly, we can consider z' as varying in the interval $[-H, H]$.

In such case, the equations of the fields radiated by a return stroke are well-known [43]; for the moment, it suffices to focus on the vertical component

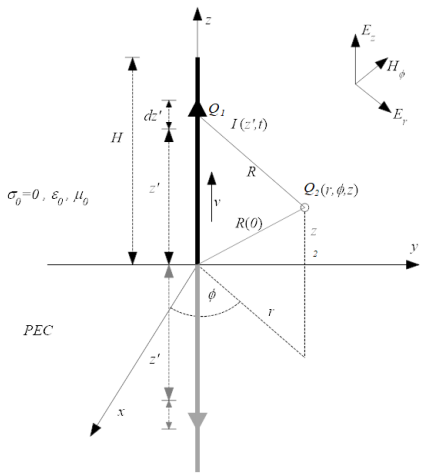

Figure 1: Geometry of the problem and corresponding coordinates.

of the electric field. Let $I(z',t)$ be the two-variable function describing the electric current in the return-stroke channel, and let us denote, for short, with "∂_t" and "R" the partial derivative with respect to t and the distance (2), respectively: then, such component is given by

$$\begin{aligned} E_z(r,z,t) = \frac{1}{4\pi\varepsilon_0}\int_{-H}^{H}\Bigg[&\frac{2(z-z')^2-r^2}{cR^4}\,I\left(z',t-\frac{R}{c}\right)\\ &-\frac{r^2}{c^2R^3}\,\partial_t I\left(z',t-\frac{R}{c}\right)\\ &+\frac{2(z-z')^2-r^2}{R^5}\int_0^t I\left(z',\tau-\frac{R}{c}\right)d\tau\Bigg]\,dz'. \end{aligned} \tag{3}$$

Its FT has been computed in [42] and it is (for $\omega \neq 0$):

$$\begin{aligned} \hat{E}_z(r,z,\omega) = \int_{-H}^{H}\Bigg[&\frac{\left(2(z-z')^2-r^2\right)\left(c^2+j\omega cR\right)}{4\pi\varepsilon_0\, j\omega c^2R^5}\\ &+\frac{\omega^2r^2R^2}{4\pi\varepsilon_0\, j\omega c^2R^5}\Bigg]\cdot e^{-\frac{j\omega R}{c}}\,\hat{I}(z',\omega)\,dz', \end{aligned} \tag{4}$$

where the following standard definition and notation for the FT of a function $f(t)$ is adopted:

$$[\mathcal{F}(f)](\omega) = \hat{f}(\omega) = \int_{-\infty}^{+\infty} f(t)e^{-j\omega t}dt, \tag{5}$$

with j being the imaginary unit.

In practice, however, any field can only be measured during a time window of finite duration. Therefore, in general, definition (5) is not applicable and the integration is to be performed over a finite time-interval. A framework addressing this problem has been presented in [41] and can be summarized as follows.

First, we can assume that the current begins to flow in the return-stroke channel at time $t_0 = 0$ and that the function $I(z', t)$ describing it has a compact support in time, i.e., that there exists $T_0 > 0$ such that

$$I(z', t) = 0 \quad \forall t \notin [0, T_0], \quad \forall z' \in [-H, H]. \tag{6}$$

A typical choice is

$$T_0 = H/v + T_c, \quad \text{with } [0, T_c] = \operatorname{supp} I(0, \cdot), \tag{7}$$

where v is the (average) speed of the return stroke (cf. (1) above) and T_c is the duration of the channel-base current $I(0, t)$.

Second, we assume that the field is measured in the time window $[0, T]$, i.e., we introduce the windowed field

$$E_z^T(r, z, t) := W_T(t) \cdot E_z(r, z, t), \tag{8}$$

where $W_T : \mathbb{R} \to \mathbb{R}$ is the time-window function defined as $W_T(t) = 1$ if $t \in [0, T]$ and $W_T(t) = 0$ otherwise. Then, from (3) and (5), and by interchanging the integrals in dz and dt, we find the following expression for the FT of (8):

$$\begin{aligned}
\hat{E}_z^T(r, z, \omega) &= \int_0^T E_z^T(r, z, t) e^{-j\omega t}\, dt \qquad (9)\\
&= \int_{-H}^{H} \left\{ \frac{2(z - z')^2 - r^2}{4\pi\varepsilon_0 c R^4} \int_0^T I\left(z', t - \frac{R}{c}\right) e^{-j\omega t}\, dt \right.\\
&- \frac{r^2}{4\pi\varepsilon_0 c^2 R^3} \int_0^T \partial_t I\left(z', t - \frac{R}{c}\right) e^{-j\omega t}\, dt\\
&\left. + \frac{2(z-z')^2 - r^2}{4\pi\varepsilon_0 R^5} \int_0^T \left[\int_0^t I\left(z', \tau - \frac{R}{c}\right) d\tau \right] e^{-j\omega t}\, dt \right\} dz'.
\end{aligned}$$

Third, in [41] it is proved that if T is chosen large enough, i.e., such that, for a fixed observation point $Q_2(r, z)$,

$$T \geq T_0 + \frac{M}{c}, \quad \text{with } M := \max_{z'} R(z') \tag{10}$$

(typically, $M = R(H)$), then (9) can be equivalently expressed, for $\omega \neq 0$, in the form

$$\hat{E}_z^T(r,z,\omega) = \int_{-H}^{H} \frac{[2(z-z')^2 - r^2]c - j\omega r^2 R}{4\pi\varepsilon_0 c^2 R^4} e^{-\frac{j\omega R}{c}} \hat{I}(z',\omega)\, dz'$$

$$+ \int_{-H}^{H} \frac{2(z-z')^2 - r^2}{4\pi\varepsilon_0 j\omega R^5} \left[e^{-\frac{j\omega R}{c}} \hat{I}(z',\omega) - e^{-j\omega T} \hat{I}(z',0) \right] dz', \tag{11}$$

provided that the channel-base current $I(0,t)$ is measured during the whole interval $[0, T_c]$, introduced above in (7). An equation analogous to (11) holds true for the radial component $\hat{E}_r^T(r,z,\omega)$ [41], but it is not reported here, since for $z = 0$ (i.e., in the case of a sensor in Q_2 at ground level, as we shall assume in Subsection 3.1) its right-hand side (RHS) vanishes identically.

Finally, the FT of the azimuthal component of the magnetic field is given by [42, 41]:

$$\hat{H}_\phi^T(r,z,\omega) = \int_{-H}^{H} \frac{cr + j\omega rR}{4\pi cR^3} \cdot e^{-\frac{j\omega R}{c}} \hat{I}(z',\omega)\, dz'. \tag{12}$$

2.2. Position of the inverse problem

In order to apply the results of [41] to the analysis of interest in this paper, we describe the return stroke by means of an MTL model, whereby a current pulse, starting from the channel base (at time $t_0 = 0$), flows upward with an (average) speed v while its intensity decreases as $|z'|$ increases, according to an (even) attenuation function $P(z')$ satisfying the initial condition $P(0) = 1$. Then, for all $(z',t) \in [-H,H] \times \mathbb{R}$, the channel current is represented by relation (1), which can be simplified, by assuming $I(0,t) = 0\ \forall t \leq 0$, in the form

$$I(z',t) = P(z')\, I\left(0, t - \frac{|z'|}{v}\right) \quad \forall (z',t) \in [-H,H] \times \mathbb{R}. \tag{13}$$

The FT of (13), as computed in [36], is given by

$$\hat{I}(z',\omega) = P(z')\, \hat{I}(0,\omega)\, \exp\left(-j\omega \frac{|z'|}{v}\right). \tag{14}$$

By substituting (14) into (11) and (12), we respectively find, for $\omega \neq 0$,

$$\hat{E}_z^T(r,z,\omega)=\hat{I}(0,\omega)\int_{-H}^{H}\left\{\frac{[2(z-z')^2-r^2]c-j\omega r^2 R}{4\pi\varepsilon_0 c^2 R^4}e^{-j\omega\left(\frac{R}{c}+\frac{|z'|}{v}\right)}\right.$$
$$\left.+\frac{2(z-z')^2-r^2}{4\pi\varepsilon_0 j\omega R^5}\left[e^{-j\omega\left(\frac{R}{c}+\frac{|z'|}{v}\right)}-e^{-j\omega T}\frac{\hat{I}(0,0)}{\hat{I}(0,\omega)}\right]\right\}P(z')\,dz', \qquad (15)$$

with $\hat{I}(0,\omega)\neq 0$, and

$$\hat{H}_\phi^T(r,z,\omega)=\hat{I}(0,\omega)\int_{-H}^{H}\frac{cr+j\omega rR}{4\pi cR^3}\,e^{-j\omega\left(\frac{R}{c}+\frac{|z'|}{v}\right)}P(z')\,dz'. \qquad (16)$$

In principle, the linear inverse problem to solve is now formulated in (15)–(16) and consists in determining the attenuation function $P(z')$ from the knowledge of $\hat{I}(0,\omega)$, $\hat{E}_z^T(r,z,\omega)$ and/or $\hat{H}_\phi^T(r,z,\omega)$, as well as of the parameters r, z, H and v. A computational approach to solve this problem will be outlined in the following.

Before that, some comments about assumptions (6) and (10), which are at the basis of our approach, are in order. Their physical meaning is that the field is measured for the whole time taken by the return-stroke current to travel up and vanish along the channel, as well as to propagate its radiation from the channel itself to the sensor at Q_2. In general, such requirement cannot be fulfilled without detecting spurious signals, since as soon as the front-wave of the current pulse reaches the top of the channel at time H/v, physical phenomena may occur which are not taken into account by the TL-type models considered here. Then, the problem arises to identify a class of return-stroke models for which the measurement time of the fields can be extended up to an instant T verifying the lower bound given by (10), so that our framework and, in particular, equations (15) and (16) are properly justified.

To this end, we observe that in most TL-type models the attenuation function $P(z')$ is decreasing and such that $P(H)$ vanishes (approximately or exactly) [40], except for the trivial and less realistic case of constant $P(z')\equiv 1$. But, if $P(H)\approx 0$, then the current at the top of the stroke channel is very small or zero, and we can expect that no meaningful electromagnetic process occurs there: while flowing upward, the current pulse originated from $z'=0$

releases a (positive) electric charge to neutralize the (negative) charge in the corona sheath surrounding the stepped leader channel [44], thus diminishing in intensity and becoming very small or vanishing for $z' = H$. In such case, we would be justified in measuring both the fields and the channel-base current until a time T such that condition (10) is satisfied. Therefore, in the following, we shall focus on MTL models such that $P(H) \approx 0$.

2.2.1. Brief hints about possible different formulations of the inverse problem

All the current-field equations (3)–(4), (9), (11)–(12), (15)–(16) considered above, both in the time and in the frequency domains, are exact in that they do not rely on any far-field approximation. However, if the far-field approximation is adopted, the current-field equations can be notably simplified and the problem of reconstructing the attenuation function from far-field data takes on specific features resulting from this simplification: see, e.g., [35] and references therein.

Moreover, it should be mentioned that, in general, the channel current may undergo not only attenuation, but also distortion; when the latter is to be taken into account, the simple model (13) for the current $I(z', t)$ should be replaced by a more sophisticated one, which can be expressed in the following form [35, 44]:

$$I(z', t) = \begin{cases} P(z')\, F\left[z', t - |z'|/v_{av}(z')\right] & \text{if } t > |z'|/v_{av}(z') \\ 0 & \text{otherwise,} \end{cases} \tag{17}$$

where $v_{av}(z') = z' / \int_0^{z'} v^{-1}(z)\, dz$ is the average speed of the return stroke from $z' = 0$ to a generic $z' > 0$ (expressed as a functional of the instantaneous speed $v(z')$), $P(z')$ is the usual attenuation function and $F(z', t)$ is a function that encodes the information about the waveshape of the current. In turn, $F(z', t)$ can be expressed in terms of a time convolution between the channel-base current $I(0, t)$ and a dispersion function $R(z', t)$ describing the modification of the current waveshape as it propagates upwards.

Now, if appropriate models and parameters for $R(z', t)$ and $v(z')$ are assumed a priori, as in [44], the inverse problem of determining the unknown function $P(z')$ from measurements of the radiated fields and of the channel-base current becomes analytically more complex than that formulated in (15)–(16), but it is still linear in $P(z')$; therefore, it should be solvable by adopting methods and techniques similar to those explained in the following Section 3. Actually, the formal analogy between the two problems consists

in the fact that the known function $I\,(0, t - |z'|/v)$ in (13) is replaced by another known function, i.e., $F\,[z', t - |z'|/v_{av}(z')]$, in (17). On the other hand, if both $P(z')$ and $F(z', t)$ are unknown, it is more reasonable to assume directly $I(z', t)$ (in the time domain) or $I(z', \omega)$ (in the frequency domain) as the unknown of the problem, which then does not fall within our framework anymore.

3. Numerical treatment

3.1. Discretization of the integral equations

A computationally efficient strategy to solve our inverse problem requires a discretization process, whereby, depending on the available fields, the integral equations (15) and/or (16) are transformed into algebraic linear systems. Such process can be implemented as described in [40] (to which we refer for more details), with some obvious modifications due to the fact that (4) has now been replaced by (11).

In short, the first step is to approximately represent the unknown function $P(z')$ as a linear combination of N suitable and known "basis functions", i.e., in the form

$$P(z') \approx \sum_{n=1}^{N} p_n\, \varphi_n(z') \quad \forall z' \in [-H, H], \tag{18}$$

where $p_n \in \mathbb{R}$ are the coefficients of the combination. Although approximate, the equality in (18) can be arbitrarily refined by increasing N, since the exact equality holds as $N \to +\infty$; then, from now on, all the equations following from (18) will be indicated as exact equalities. In any case, we shall see that, for our purposes, N can be profitably chosen as not larger than 12. Since $P(0) = 1$, the coefficients p_n verify the "normalization condition"

$$\sum_{n=1}^{N} p_n\, \varphi_n(0) = 1. \tag{19}$$

Now, let us focus on (15), since analogous considerations and notation are valid for (16): the RHS of (15) can be regarded as the action of a linear integral operator $A_{z,1}$ (acting between proper spaces of square-integrable functions) on $P(z')$. The number 1 in the subindex of $A_{z,1}$ is used to distinguish the integral operator associated with (15) from its counterpart in (16),

$A_{z,2}$. By linearity and (18), relation (15) can be written in compact form as

$$\hat{I}(0,\omega)\sum_{n=1}^{N} p_n\big[A_{z,1}\big(\varphi_n\big)\big](r,\omega) = \hat{E}_z^T(r,z,\omega). \tag{20}$$

Moreover, if we set $\lambda(\omega) = 1/\hat{I}(0,\omega)$ (not to be confused with any wavelength) and $g_1(r,z,\omega) = \hat{E}_z^T(r,z,\omega)$, we can express (20), as well as the analogous relation following from (16) with $g_2(r,z,\omega) = \hat{H}_\phi^T(r,z,\omega)$, in the form

$$\sum_{n=1}^{N} p_n\big[A_{z,i}\big(\varphi_n\big)\big](r,\omega) = \lambda(\omega) g_i(r,z,\omega), \quad i = 1,\, 2. \tag{21}$$

In general, measurements can be taken at various horizontal distances r_s from the return-stroke channel, labeled by the index $s = 1,\ldots,S$, and considered at different angular frequencies $\omega_{s,f}$, labeled by the sensor index s and the frequency index $f = 1,\ldots,F(s)$; accordingly, analogous labels also apply to $\lambda_{s,f} = \lambda\left(\omega_{s,f}\right)$. In realistic applications, S is small, since it coincides with the number of field sensors, whereas $F(s)$ is large for any sensor s, since the channel-base current and the fields are usually measured in the time domain and then Fourier-transformed by means of computations, such as FFT, that usually involve a large number of frequencies. Moreover, sensors are typically at ground level, so that we can assume $z = 0$.

Hence, if we define the $\left(\sum_{s=1}^{S} F(s) + 1\right) \times N$ matrix

$$\mathbf{R}_i = \left[\begin{array}{ccc}
\big[A_{0,i}\big(\varphi_1\big)\big]\big(r_1,\omega_{1,1}\big) & \cdots & \big[A_{0,i}\big(\varphi_N\big)\big]\big(r_1,\omega_{1,1}\big) \\
\vdots & \vdots & \vdots \\
\big[A_{0,i}\big(\varphi_1\big)\big]\big(r_1,\omega_{1,F(1)}\big) & \cdots & \big[A_{0,i}\big(\varphi_N\big)\big]\big(r_1,\omega_{1,F(1)}\big) \\
\hdashline
\vdots & \vdots & \vdots \\
\hdashline
\big[A_{0,i}\big(\varphi_1\big)\big]\big(r_S,\omega_{S,1}\big) & \cdots & \big[A_{0,i}\big(\varphi_N\big)\big]\big(r_S,\omega_{S,1}\big) \\
\vdots & \vdots & \vdots \\
\big[A_{0,i}\big(\varphi_1\big)\big]\big(r_S,\omega_{S,F(S)}\big) & \cdots & \big[A_{0,i}\big(\varphi_N\big)\big]\big(r_S,\omega_{S,F(S)}\big) \\
\hdashline
\varphi_1(0) & \cdots & \varphi_N(0)
\end{array}\right], \tag{22}$$

we can assemble (21) and (19) into an algebraic linear system in matrix form

for the unknown vector $[p_1, \ldots, p_N]^{\mathrm{T}}$, i.e.,

$$\mathbf{R}_i \begin{bmatrix} p_1 \\ \vdots \\ p_N \end{bmatrix} = \begin{bmatrix} \lambda_{1,1}\, g_i\big(r_1, 0, \omega_{1,1}\big) \\ \vdots \\ \lambda_{1,F(1)}\, g_i\big(r_1, 0, \omega_{1,F(1)}\big) \\ \vdots \\ \lambda_{S,1}\, g_i\big(r_S, 0, \omega_{S,1}\big) \\ \vdots \\ \lambda_{S,F(S)}\, g_i\big(r_S, 0, \omega_{S,F(S)}\big) \\ 1 \end{bmatrix}, \quad i = 1,\, 2. \tag{23}$$

Moreover, if both sets of measurements $i = 1$ (electric field) and $i = 2$ (magnetic field) are available, the two corresponding systems in (23) can be unified into a single one, by replacing the matrix $\mathbf{R}_i$ with the $\Big(2\sum_{s=1}^{S} F(s) + 1\Big) \times N$ matrix $\mathbf{R} = [\mathbf{R}_1', \mathbf{R}_2]^{\mathrm{T}}$, where the block $\mathbf{R}_1'$ is obtained from $\mathbf{R}_1$ by canceling its last row; clearly, the RHS of (23) should undergo an analogous rearrangement, and the resulting system could be written in compact form as

$$\mathbf{R} \begin{bmatrix} p_1 \\ \vdots \\ p_N \end{bmatrix} = \begin{bmatrix} \lambda_{1,1}\, g_1\big(r_1, 0, \omega_{1,1}\big) \\ \vdots \\ \lambda_{S,F(S)}\, g_2\big(r_S, 0, \omega_{S,F(S)}\big) \\ 1 \end{bmatrix}. \tag{24}$$

Finally, since the entries of the matrices $\mathbf{R}_i$ and the components of the free term on the RHS of (23) are complex numbers, the natural space of solutions for such system would be $\mathbb{C}^N$, whereas the unknown coefficients p_n are real. The latter requirement is easily enforced, from an algorithmic viewpoint, by splitting (23) into its real and imaginary parts, thus obtaining a system of double dimension (more precisely, of $2\sum_{s=1}^{S} F(s) + 1$ equations, since the last row of $\mathbf{R}_i$ is real) to be solved in $\mathbb{R}^N$. Of course, the same strategy can be applied to the unified system (24).

3.2. Computation of noiseless data

After having deduced the algebraic structure (22)–(24) of the discretized inverse problem, we now describe the computation of the data, i.e., of the matrices $\mathbf{R}_i$, $\mathbf{R}$ and of the free terms of systems (23)–(24). The procedure can be split into the following steps:

1) choice of the basis functions φ_n and their number N: as regards the former, we pick the Gegenbauer polynomials of order $s = 1/2$ [38, 40]; as regards the latter, numerical simulations presented subsequently in Subsection 4.1 suggest that $N = 12$ is sufficient for any practical purpose;
2) choice of some realistic parameters appearing in the formulation of the problem: in our simulations, except when explicitly stated otherwise, we set $H = 4.0\,\mathrm{km}$, $v = c/2 = 1.5 \cdot 10^8\,\mathrm{m/s}$, $S = 1$, $r = r_1 = 5.0\,\mathrm{km}$, $T_c = 1000\,\mu\mathrm{s}$ and, by (7), (10),

$$T = T_c + H/v + R(H)/c \approx 1048\,\mu\mathrm{s}. \tag{25}$$

Since the sensor is only one, in the following we shall omit the sensor subindex s by simply writing r, ω_f and λ_f;
3) choice of the attenuation function: among the various possibilities [40], we pick: a) $P(z') = e^{-|z'|/\lambda}$, with $\lambda = 2000\,\mathrm{m}$ (MTLE model); b) $P(z') = 1 - z'/H$ (MTLL model); c) $P(z') = 1 - (z'/H)^2$ ("quadratic model"). The attenuation functions of a) and b) belong to a set of well-established models, whereas c) is an additional model introduced by us to make some more tests;
4) choice of a realistic model for the current $I(0,t)$ at the base of the return-stroke channel: to this end, we use the Heidler's function [29]

$$I_H(t) = I_S \frac{(t/\tau_1)^n}{1 + (t/\tau_1)^n} \exp\left[-\frac{t}{\tau_2} + \frac{\tau_1}{\tau_2}\left(n\frac{\tau_2}{\tau_1}\right)^{\frac{1}{n}}\right], \tag{26}$$

with the following values of the parameters, typical of a first return-stroke: $I_S = 28.215\,\mathrm{kA}$, $\tau_1 = 1.8\,\mu\mathrm{s}$, $\tau_2 = 95\,\mu\mathrm{s}$, $n = 2$ [45];
5) computation of a discretized version of $\hat{I}(0,\omega)$ via FFT: such step also requires the choice of some parameters (e.g., the number F of frequencies), but this point will be discussed later, in Subsection 3.3. As a result, we determine both $\hat{I}(0,\omega_f)$ and $\lambda_f = 1/\hat{I}(0,\omega_f)$, for $f = 1, \ldots, F$;
6) computation of a discretized version of $\hat{E}_z^T(r,0,\omega)$ and/or $\hat{H}_\phi^T(r,0,\omega)$: both to avoid any inverse crime [46] and to reproduce the realistic situation where the fields are first measured (and affected by noise, cf. Subsection 3.3) in the time domain and then Fourier transformed, we do not compute $\hat{E}_z^T(r,z,\omega_f)$ and/or $\hat{H}_\phi^T(r,z,\omega_f)$ via (15)–(16), but rather we substitute the Heidler's function modeling $I(0,t)$ into the time-domain equation (3) (and/or into the analogous one for the magnetic field), then we numerically compute a discretized version of $E_z(r,0,t)$ and/or $H_\phi(r,0,t)$, and finally

we apply the FFT to the latter in order to determine $\hat{E}_z^T(r,0,\omega_s)$ and/or $\hat{H}_\phi^T(r,0,\omega_s)$. Again, the parameters used to implement the FFT algorithm will be discussed in Subsection 3.3. As a result of steps 5) and 6), the computation of the free terms on the RHSs of (23)–(24) is complete;

7) computation of the entries of the matrices $\mathbf{R}_i$, $\mathbf{R}$: once the basis functions φ_n have been chosen as in step 1), the entries $\big[A_{0,i}\big(\varphi_n\big)\big](r,\omega_f)$ of the matrices $\mathbf{R}_i$, $\mathbf{R}$ can be determined by numerically computing the integrals in dz' appearing on the RHSs of (15)–(16).

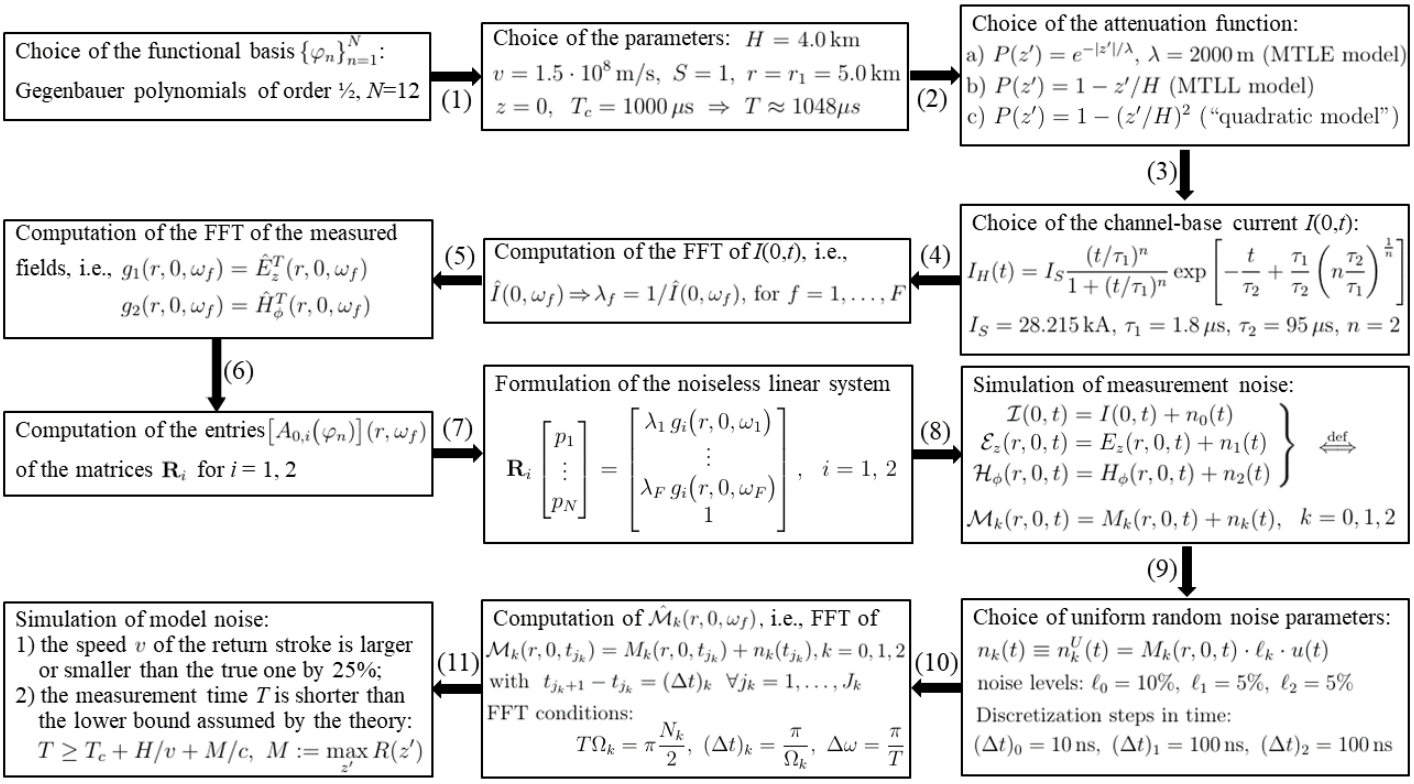

Figure 2: Block diagram summarizing the content of Subsections 3.2–3.4.

In the previous steps 1)–7), we have outlined the procedure adopted by us to compute all the noiseless data necessary for an explicit formulation of systems (23)–(24). However, in order to simulate realistic situations, this procedure should be completed with some further steps, which include the effect of noise. The description of such steps is presented in the next two

subsections. In order to favor readability, the content of Subsections 3.2–3.4 is schematically illustrated in the block diagram of Fig. 2; so far, we have described the blocks (1) to (8) of the diagram. The remaining ones will be described in the next two subsections.

3.3. Simulation of measurement noise

Any real measurement of a current or a field is inevitably affected by noise. Since these measurements are typically made in the time domain, adding noise directly to the FTs of the channel-base current and of the fields would not be appropriate; rather, we should first consider a realistic noise-model in the time domain, so as to reproduce the noisy data

$$\mathcal{I}(0,t) = I(0,t) + n_0(t), \tag{27}$$

$$\mathcal{E}_z(r,0,t) = E_z(r,0,t) + n_1(t), \tag{28}$$

$$\mathcal{H}_\phi(r,0,t) = H_\phi(r,0,t) + n_2(t), \tag{29}$$

and then compute their FTs, in order to obtain the noisy frequency-domain data $\hat{\mathcal{I}}(0,\omega)$, $\hat{\mathcal{E}}(r,0,\omega)$ and/or $\hat{\mathcal{H}}_\phi(r,0,\omega)$. In (27)–(29), the functions $n_k(t)$, with $k = 0,1,2$, describe the noise affecting the quantities to be measured. If we denote by $M_k(r,0,t)$, for $k = 0,1,2$, the functions $I(0,t)$, $E_z(r,0,t)$ $H_\phi(r,0,t)$ respectively, we can summarize (27)–(29) in the form

$$\mathcal{M}_k(r,0,t) = M_k(r,0,t) + n_k(t), \quad k = 0,1,2. \tag{30}$$

Here, we consider two frequently used noise models:
1) Gaussian noise: given a noise level $\ell_k \in [0,1]$, we define

$$n_k(t) \equiv n_k^G(t) = M_k(r,0,t) \cdot \ell_k \cdot g(t), \tag{31}$$

where, for each $t \in [0,T]$, the scalar $g(t)$ is the realization of a random variable distributed according to the normal distribution $\mathcal{N}(\mu,\sigma^2)$, with mean $\mu = 0$ and standard deviation $\sigma = \frac{1}{3}$, so that such realization falls in the interval $[-1,1]$ in essentially all cases (more precisely, in $99,73\%$ of them);
2) uniform random noise: given a noise level $\ell_k \in [0,1]$, we define

$$n_k(t) \equiv n_k^U(t) = M_k(r,0,t) \cdot \ell_k \cdot u(t), \tag{32}$$

where, for each $t \in [0,T]$, the scalar $u(t)$ is the realization of a random variable distributed according to the uniform distribution $\mathcal{U}(-1,1)$ in the interval $[-1,1]$.

So far, for the sake of simplicity, we have outlined the scheme of noise simulation as if we worked in a continuous framework, but some more detail is required if we want to deal with a discretized setting. Taking inspiration from the experimental setup described in [47], we assume that each measurement in the time-domain is characterized not only by its accuracy (which can be identified with the noise level ℓ_k), but also by a certain time resolution $(\Delta t)_k$ (which can be identified with the discretization step in time). More precisely, according to the measurements performed in [47], the noise levels and the discretization steps should be respectively chosen as $(\Delta t)_0 = 10\,\text{ns}$, $\ell_0 = 10\%$ for the channel-base current $I(0,t)$, and $(\Delta t)_1 = 100\,\text{ns}$, $\ell_1 = 5\%$ for the electric field $E_z(r,0,t)$. Since no magnetic field is measured in [47], by mere analogy we also choose $(\Delta t)_2 = 100\,\text{ns}$, $\ell_2 = 5\%$ for $H_\phi(r,0,t)$. As a result, the current and the fields are considered for a finite number J_k of time instants t_{j_k} such that $t_{j_k+1} - t_{j_k} = (\Delta t)_k$ for all $j_k = 1, \ldots, J_k$, and the corresponding discretized version of (30) can be written as

$$\mathcal{M}_k(r,0,t_{j_k}) = M_k(r,0,t_{j_k}) + n_k(t_{j_k}), \quad k = 0,1,2. \tag{33}$$

As regards the case $k = 0$, it suffices to discretize the Heidler's function, i.e., to set $M_0(r,0,t_{j_0}) = I_H(t_{j_0})$ for $j_0 = 1, \ldots, J_0$. As regards the case $k = 1$, we first consider a ten times sparser discretization of the Heidler's function, i.e., $I_H(t_{j_1})$, and then we substitute it in the time-domain equation (3), where the integrals are computed via the trapezoidal rule; as a result, we obtain the discretized electric field $M_1(r,0,t_{j_1})$ for $j_1 = 1, \ldots, J_1$. The case $k = 2$ is treated analogously to the case $k = 1$.

We should now compute the FFT of $\mathcal{M}_k(r,0,t_{j_k})$ for each $k = 0,1,2$. To this end, we first recall, in general, the (not all independent) conditions ensuring that the FFT is a discretization of the FT [48]:

$$T\Omega = \pi\frac{N}{2}, \quad \Delta t = \frac{\pi}{\Omega}, \quad \Delta\omega = \frac{\pi}{T}, \quad \Delta t \cdot \Delta\omega = \frac{2\pi}{N}, \tag{34}$$

where $[-T,T]$ is the time window and $[-\Omega,\Omega]$ the corresponding (angular) frequency window, N is the number of equispaced samples both in the time and the frequency domain, whereas $\Delta t = 2T/N$ and $\Delta\omega = 2\Omega/N$ are the distances between two consecutive samples in the two domains, respectively.

Now, when considered with reference to (33), in principle all the parameters appearing in (34), as well as the number of samples $J_k = 2T_k/(\Delta t)_k$, depend on k, since the channel-base current and the fields might well be

measured with different time resolutions, as in [47], and in different time-windows. However, in such case, the sets of discrete frequencies at which the FFTs of the current and the fields are computed would also be different, and this might impair the formulation of systems (23)–(24), which require a common set of frequencies to be considered for the current and the fields.

The impact of such problem can be controlled by adopting the following strategy. As regards the difference among time resolutions $(\Delta t)_k$, this implies a corresponding difference among the maximum frequencies $\Omega_k = \pi/(\Delta t)_k$ achievable by the FFT; accordingly, it suffices to consider only the frequencies not larger than the minimum of the values Ω_k. As regards the difference among time windows, i.e., among T_k, this implies a corresponding difference among the discretization steps in the frequency domain, i.e., $(\Delta\omega)_k = \pi/T_k$. Hence, we set in our simulations, first of all, $T_1 = T_2 = T$, i.e., we assume that the electric and magnetic fields are measured in the same time window. Moreover, by (7), the channel-base current vanishes for $t > T_c$, then we can easily assume that also this current is measured in the same time window as the fields, thus replacing the natural interval $[-T_c, T_c]$ with $[-T, T]$.

However, the latter trick deserves some further comment. As claimed in step 4) of Subsection 3.2, we choose the Heidler's function $I_H(t)$ as a model for $I(0, t)$. Nevertheless, such function never vanishes, but only tends asymptotically to zero as t increases. Then, in principle, we should modify $I_H(t)$ in such a way that $I_H(t) = 0$ for all $t \in [T_c, T]$ and $I_H(t)$ is derivable in $[0, T]$ (cf. the term with $\partial_t I$ in the second line of (3)). However, for $t > T_c$ the values of the functions $I_H(t)$ and $\partial_t I_H(t)$ are extremely small, so that the error made when $I_H(t)$ is maintained unaltered in the whole interval $[0, T]$ should be negligible and comparable to other numerical errors due to approximation and discretization procedures implemented in the code: all of them should be effectively treated by regularization techniques. Such conjecture is confirmed by the simulations and reconstructions that will be presented in Subsection 4.1, where the function $I_H(t)$ is used in the interval $[0, T]$ without changes. For this reason, the same procedure is adopted in Subsection 4.2.

3.4. Simulation of model noise

In addition to measurement noise, model noise should also be taken into account in real applications, since the underlying parameters or assumptions characterizing the model adopted to formulate the equations of the inverse

problem are known or fulfilled only with a certain degree of approximation. Among the many possible discrepancies, a priori conceivable, between our model and a realistic measurement record, we decided to focus on two specific circumstances, which correspond to either an inaccurate parameter knowledge or a restrictive condition, i.e.,

1) the speed v of the return stroke is larger or smaller than the true one: for example, in [47] it is claimed that v is measured with accuracies ranging from 15% to 25%;

2) the measurement time T is shorter than the lower bound established by (10), as occurs, again, in [47].

It is expected that, within certain limits, the impact of these discrepancies is attenuated by regularization methods. The results presented in Subsection 4.2 support this claim.

In our framework, an at least approximate knowledge of the return-stroke speed v is necessary. Unfortunately, in most of practical cases, v is simply unknown. However, our approach can still be adopted by referring to the statistical variations of v [49].

3.5. Inversion and regularization

The last numerical step consists in solving the inverse problem of interest, i.e., the linear system (23) or (24), by means of an appropriate regularization procedure that can effectively treat its ill-posedness. In real measurements, where no "exact" data are available, it is very difficult, if not impossible, to estimate the level of the noise affecting the matrices $\mathbf{R}_i$, $\mathbf{R}$ and the free terms of systems (23)–(24). To cope with this problem, we only consider the so-called *heuristic* methods [50] as eligible regularization techniques, since they do not require any a priori information about noise. More specifically, we found that the well-known Tikhonov regularization, coupled with the L-curve method [51] for the computation of the regularization parameter, provides satisfactory results in very short times (a few seconds on a common laptop). The implementation of this algorithm is made easy by the routines of the MATLAB package described in [52].

The only point worth discussing here concerns the choice of the frequencies ω_f to be considered in the formulation of systems (23)–(24). As a heuristic criterion, we observe that for lower frequencies, the spectra of the channel-base current and of the fields are both more intense and less affected by noise than for higher frequencies, as shown in Fig. 3; accordingly, a reasonable strategy might consist in working with the first F lower frequencies,

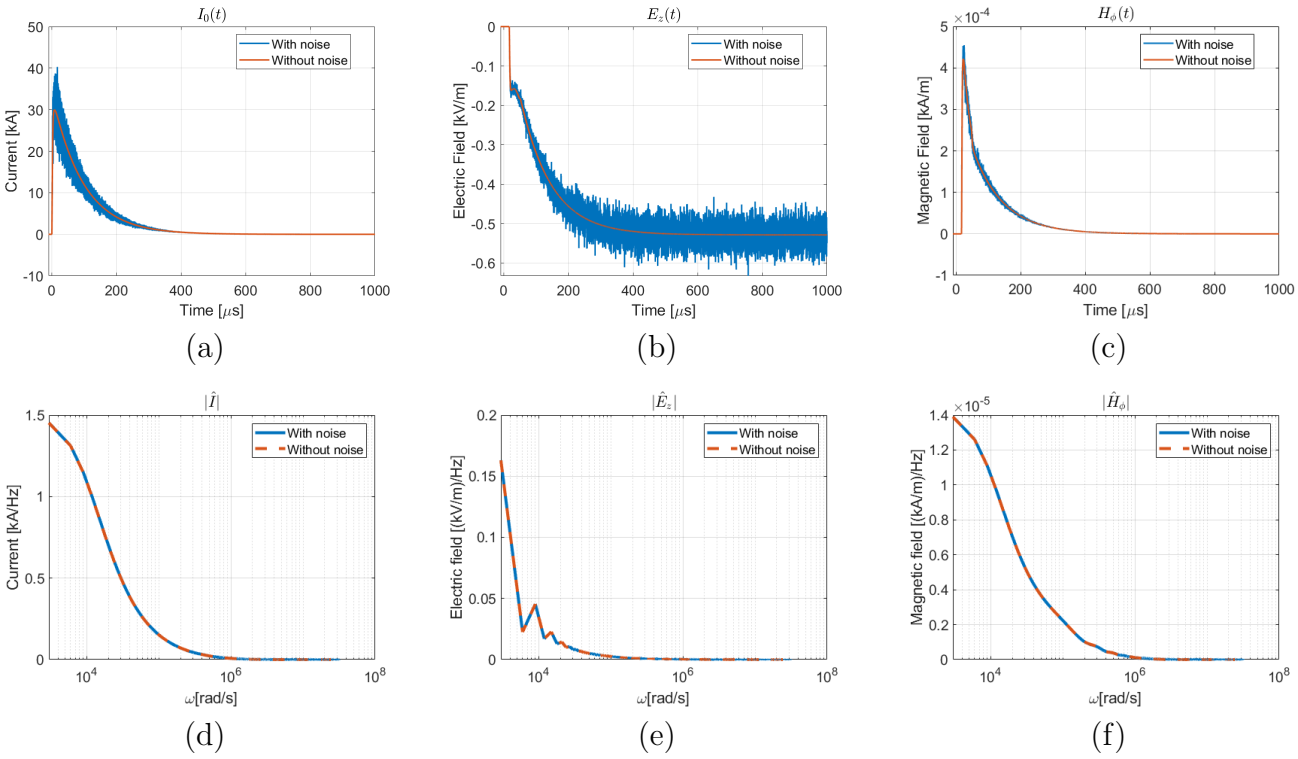

Figure 3: Plots of (a) the channel-base current $I(0,t)$, (b) the electric field $E_z^T(r,0,t)$, (c) the magnetic field $H_\phi^T(r,0,t)$ and their respective spectra (d)-(f), obtained by using the MTLE model, with the following values of the parameters: measurement time $T = 1048\,\mu$s; channel height $H = 4.0\,$km, return-stroke speed $v = 1.5{\cdot}10^8\,$m/s, horizontal distance of the sensor from the channel $r = 5.0\,$km. As regards panels (d)-(f), on the x-axis the frequencies ω_{j_k} are considered; the discrete values are represented via linear interpolation; the solid and dashed lines refer to noiseless data and uniform random noise data, respectively.

with F being such that the number of equations is not smaller than the number of unknowns, and, in case of a bad reconstruction, increasing F, i.e., adding some more higher and consecutive frequencies until the "best" reconstruction is obtained. Since this approach, which we pursue by simple visual inspection, yields good results, at least when an effective performance of the algorithm is expected (as shown in Fig. 5, discussed in the next section), we shall not make a deeper analysis of this issue (involving, e.g., the dependence of the condition numbers of the system matrices $\mathbf{R}_i$, $\mathbf{R}$ on the set of frequencies). However, in real applications, when the underlying exact expression of $P(z')$ is unknown and no predetermined concept of "good reconstruction" is available, such analysis might provide some useful insights.

4. Reconstruction of the attenuation function

4.1. Measurement noise

Here, we present the reconstructions obtained for the attenuation function $P(z')$ when the data are computed as explained in Subsections 3.2–3.3 and inverted as described in Subsection 3.5. In order to favor readability, a block-diagram scheme of the content of Subsections 4.1–4.2 is displayed in Fig. 4.

As regards Fig. 5, panels (a)–(c) show the reconstructions corresponding to the three possible forms of $P(z')$ considered in step 3) of Subsection 3.2, when, besides the channel-base current, only the electric field is considered; panels (d)–(f) and (g)–(i) are analogous to (a)–(c), except that the electric field is either replaced by or combined with the magnetic field, respectively. In all cases, the current and the field data are affected by a uniform random noise, but very similar results are obtained also in the case of Gaussian noise.

A comparison of the panels of each column of the first three rows in Fig. 5 suggests that, when both fields are considered as input data, no actual improvement is obtained and the impact of the electric field is stronger than that of the magnetic field; such trend is confirmed by the numerical experiments of Subsection 4.2. This is arguably due to the fact that, from a numerical viewpoint, the intensity of the FT of the electric field is around 10^4 times greater than that of the FT of the magnetic field over all the frequencies of their spectra. In order to clarify this point, let us come back to the unified system (24), which we now denote in symbolic form as $\mathbf{R}P = G$. If an exact solution of such system were to be computed, any one of its equations could be multiplied by a constant factor without consequences, but when a Tikhonov regularized solution is looked for, this is not true anymore: indeed,

Tikhonov regularization minimizes a functional such that one of its addenda is the so-called *discrepancy* $\|\mathbf{R}P - G\|$, whose values can change if one or more of the equations of the system is multiplied by some constant factor. Hence, in order to balance the contributions that each one of the two fields gives to the discrepancy, it might be useful to multiply all the magnetic-field equations of system (24) by a factor 10^4. The results obtained by adopting such rescaling strategy are shown in panels (l)–(n) of Fig. 5, which seem to indicate a more balanced influence of the two fields in producing the final reconstruction. As before, also this trend is confirmed (with more evidence) by the numerical experiments that will be presented in Subsection 4.2.

Since all these reconstructions are obtained in very short computational times from data affected by a realistic noise and are satisfactory even when based on single-field measurements, we shall not try to discuss possible improvements of the overall strategy in order to state some optimality criterion (e.g., minimum numbers of frequencies or sensors).

4.2. Model noise

As anticipated in Subsection 3.4, we now wish to test how an erroneous estimate of the speed v of the return stroke can affect the reconstruction of $P(z')$. To this end, we consider again the numerical simulations of Fig. 5: while letting all the other parameters and data unaltered, we purposely change the value of v only in the inversion procedure (i.e., in computing the entries of the matrices $\mathbf{R}_i$, $\mathbf{R}$) by decreasing such value by 25%, which should correspond to a worst-case scenario [47].

The results are displayed in Fig. 6: in spite of a clear deterioration of the reconstructions in all cases, the order of magnitude and some general features of the plots of $P(z')$ are preserved. In particular, the great similarity between the two sets of panels (a)–(c) and (g)–(i) shows that the magnetic field proves almost irrelevant when combined with the electric field without rescaling, whereas panels (l)–(n) suggest that the rescaling strategy is a more appropriate way for coupling the two fields and can probably yield the best possible results.

However, we should be careful to not extend these observed properties beyond the specific simulations performed here. In general, there are many parameters that might be varied, and a thorough statistical analysis is beyond the scope of this paper. Here, we limit ourselves to pointing out that even an error of 25% on the value of the speed v does not necessarily entail a complete loss of information on the attenuation function.

A wrong estimate of v provides an example of an error affecting one of the parameters characterizing an otherwise correct model. But we can conceive more sophisticated situations, where some underlying hypotheses of the model are not verified: this is the case, e.g., of short-time measurements, which do not fulfill assumptions (6) and (10). Actually, it could be proved that, in such case, the equations of the model need to be modified. Here, we just show, for a specific instance, the gradual deterioration of the reconstruction of $P(z')$ as the time window $[0, T]$ of the field measurement shortens.

To this end, we focus on the reconstruction of Fig. 5(a), obtained for $T_c = 1000\,\mu$s, which corresponds, by (25), to a measurement time $T = 1048\,\mu$s. While leaving all the other parameters and data unaltered, we gradually decrease T_c (and then, by (25), also $T = T_c + 48\,\mu$s): in Fig. 7 we show the results obtained for $T_c = 500\,\mu$s (panel (a)), $T_c = 300\,\mu$s (panel (b)), $T_c = 100\,\mu$s (panel (c)), $T_c = 50\,\mu$s (panel (d)), $T_c = 10\,\mu$s (panel (e)), $T_c = 5.0\,\mu$s (panel (f)).

Whereas the reconstruction of $P(z')$ is still good in panel (a), it worsens more and more throughout panels (b)–(f), in spite of regularization. The crucial point here is that the model represented by (15)–(16) becomes inadequate.

5. Conclusions

In this paper, we developed a frequency-domain framework to solve the inverse problem of reconstructing the attenuation function of the return-stroke current along the lightning channel, from the measurements of the radiated fields, the channel-base current, the channel height and the return-stroke speed. The reconstructions thus obtained (in particular, those presented in Subsection 4.1) show that such framework can be effectively applied in noisy and realistic conditions, thus supporting, in particular, the validity of the two main new elements of this paper, i.e., 1) the inversion of a discretized form of the current-field equations deduced in [41]; 2) the low-pass filtering procedure of measurement noise, as made possible by the FT of a preliminary and realistic model of this noise in the time domain, both for the fields and the channel-base current.

Nevertheless, the whole treatment is based on the assumption of long-duration time-windows, i.e., on conditions (6) and (10), which may not always be fulfilled; in particular, the measurement time T of the field may be much

shorter than the lower bound prescribed by (10). This typically happens in two cases: 1) the measurements are conceived and taken for purposes different from that of reconstructing the attenuation function $P(z')$, such as in [47]; however, using these data to recover $P(z')$ might be of interest; 2) the fulfillment of (10) could not be obtained without detecting spurious signals, thus impairing the inversion procedure.

Hence, future research should be aimed at formulating a theoretical treatment of the case where short-duration time-windows are considered and, in particular, at deducing the corresponding new current-field equations; the resulting procedure should then be tested against simulated and real data to obtain reliable reconstructions of the attenuation function.

Another interesting future development is to tackle an analogous inverse problem without measuring the channel-base current [40] (and/or the channel height [37]): this would allow considering also return strokes in natural lightning flashes (not striking instrumented towers or artificially triggered by metallic wires unrolled by rockets).

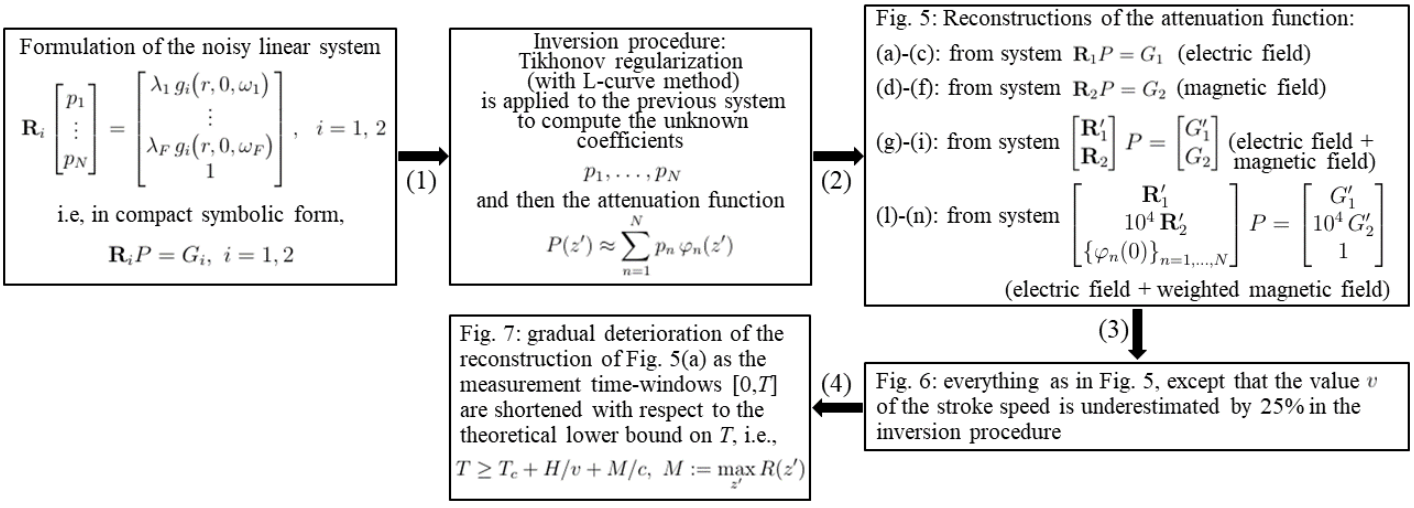

Figure 4: Block diagram summarizing the content of Subsections 4.1–4.2. Strictly speaking, the first and second blocks pertain to Subsections 3.1 and 3.5 respectively, but recalling their notation is useful to read the third block.

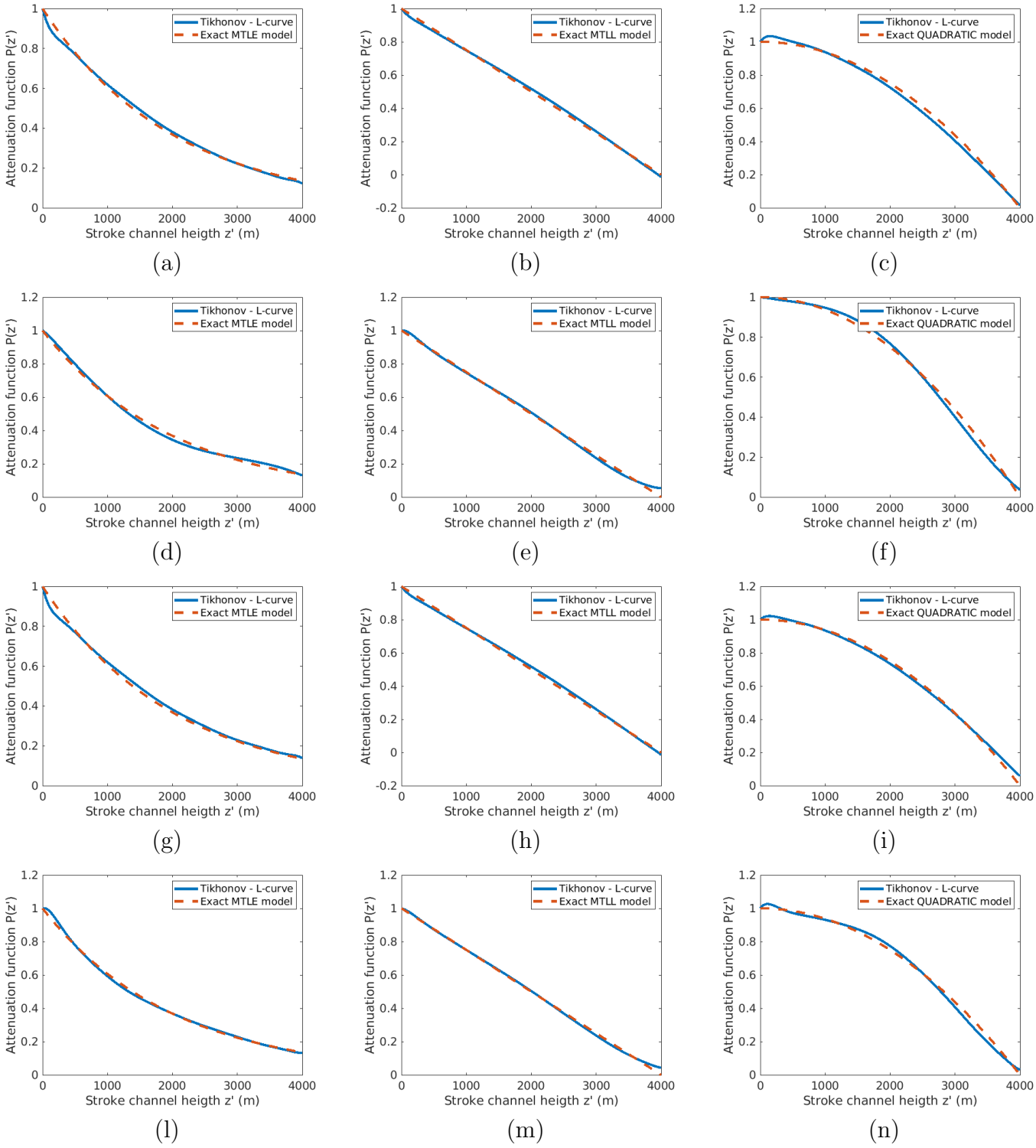

Figure 5: Plots of the reconstruction of the attenuation function $P(z')$ for three different models, i.e., MTLE (panels (a), (d), (g) and (l)), MTLL (panels (b), (e), (h) and (m)) and quadratic (panels (c), (f), (i) and (n)). The data are affected by uniform random noise, for a measurement time $T = 1048\,\mu$s. Besides the channel-base current, the measured fields are electric (panels (a)–(c)), or magnetic (panels (d)–(f)), or both (panels (g)–(i)); finally, panels (l)–(n) correspond to the case in which both fields are considered, but the magnetic-field equations are multiplied by a factor 10^4 in order to balance the contributions of the two fields in the regularization procedure. Each reconstruction is obtained by using a number F of lower frequencies, with (a) $F = 16$; (b) $F = 17$; (c) $F = 16$; (d) $F = 19$; (e) $F = 32$; (f) $F = 27$; (g) $F = 15$; (h) $F = 17$; (i) $F = 21$; (l) $F = 13$; (m) $F = 32$; (n) $F = 26$. The solid and dashed lines refer to the reconstructed and the true plots of $P(z')$, respectively.

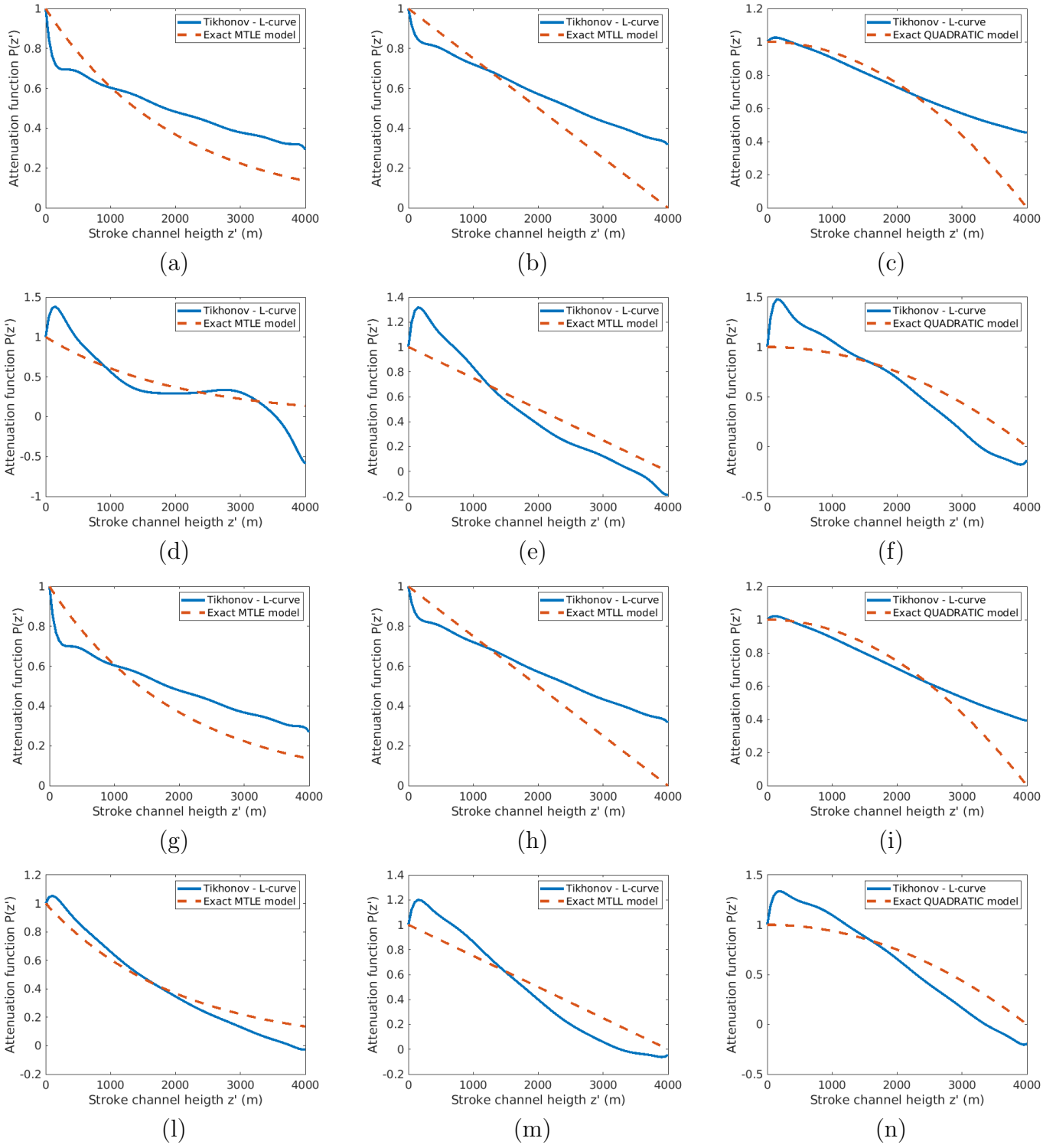

Figure 6: Everything as in Fig. 5, except that the value of the stroke speed v used in the inversion procedure is 25% less than the "true" value, i.e., the value chosen to produce the current and field data.

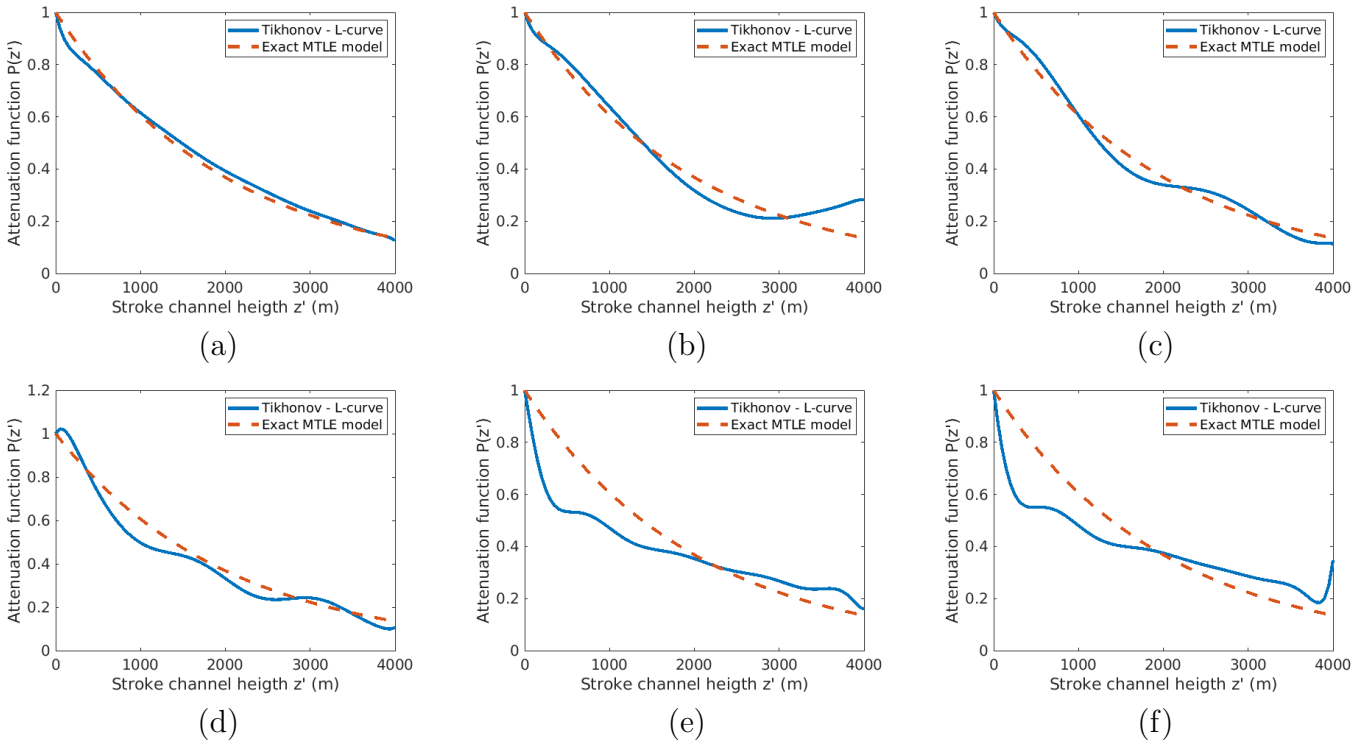

Figure 7: Gradual deterioration of the reconstruction shown in Fig. 5(a) as the measurement time-windows $[0, T]$ are shortened. We display the results obtained for $T_c = 500\,\mu$s (panel (a)), $T_c = 300\,\mu$s (panel (b)), $T_c = 100\,\mu$s (panel (c)), $T_c = 50\,\mu$s (panel (d)), $T_c = 10\,\mu$s (panel (e)), $T_c = 5.0\,\mu$s (panel (f)); by (25), the corresponding measurement times are $T = T_c + 48\,\mu$s.

Acknowledgment

This work was partially supported by the Italian Ministry for Education, University, and Research under the project PRIN2017 DI-CA, grant number 20177C3WRM.

References

[1] IEEE Draft Guide for Improving the Lightning Performance of Electric Power Overhead Distribution Lines, IEEE P1410/D7 (2010) 1–70.

[2] IEEE Guide for Improving the Lightning Performance of Transmission Lines, IEEE Std 1243-1997 (1997) 1–44.

[3] M. N. Plooster, Shock waves from line sources. Numerical solutions and experimental measurements, Phys. fluids 13 (11) (1970) 2665–2675.

[4] M. N. Plooster, Numerical simulation of spark discharges in air, Phys. fluids 14 (10) (1971) 2111–2123.

[5] S. I. Braginskii, Theory of the development of a spark channel, Sov. Phys. JETP 34 (1958) 1068–1074.

[6] R. Moini, S. H. H. Sadeghi, B. Kordi, F. Rachidi, An antenna-theory approach for modeling inclined lightning return stroke channels, Electr. Power Syst. Res. 76 (11) (2006) 945–952.

[7] R. Moini, B. Kordi, G. Z. Rafi, V. A. Rakov, A new lightning return stroke model based on antenna theory, J. Geophys. Res. Atmos. 105 (D24) (2000) 29,693–29,702.

[8] C. R. Paul, Analysis of Multiconductor Transmission Lines, 2nd Edition, John Wiley and Sons, Inc., Hoboken, NJ, 2007.

[9] J. E. Borovsky, An electrodynamic description of lightning return strokes and dart leaders: Guided wave propagation along conducting cylindrical channels, J. Geophys. Res. Atmos. 100 (D2) (1995) 2697–2726.

[10] V. Cooray, J. E. Borovsky, Electrodynamic model of lightning return stroke – spatial and temporal variation of the return stroke current, in: Proceedings of the International Symposium on Lightning Protection (XIV SIPDA), Natal, Brazil, 2017.

[11] V. Cooray, Unification of engineering return stroke models, Electr. Pow. Syst. Res. 195 (2021) 1–10.

[12] M. A. Uman, D. K. McLain, Magnetic field of lightning return stroke, J. Geophys. Res. 74 (28) (1969) 6899–6910.

[13] V. A. Rakov, A. A. Dulzon, Results of calculation of the electromagnetic fields of lightning discharges (in Russian), Tekh. Elektrodinam. 1 (1987) 87–89.

[14] C. A. Nucci, On lightning return stroke models for LEMP calculations, in: Proc. 19th Int. Conf. Lightning Protection, Graz, Austria, 1988.

[15] V. Javor, Modified Transmission Line Models of Lightning Strokes Using New Current Functions and Attenuation Factors, in: S. Silvestrov, M. Rančić (Eds.), Engineering Mathematics I, Vol. 178 of Springer Proceedings in Mathematics and Statistics, Springer, Cham (CH), 2016, pp. 131–149.

[16] V. A. Rakov, M. A. Uman, Review and Evaluation of Lightning Return Stroke Models Including Some Aspects of Their Application, IEEE Trans. Electromag. Compat. 40 (4) (1998) 403–426.

[17] F. Heidler, Traveling current source model for LEMP calculation, in: Proc. 6th Int. Zurich Symp. Electromagnetic Compatibility (1985-3), Swiss Fed. Inst. of Technol., Zurich, Switzerland, 1985, pp. 157–162.

[18] G. Diendorfer, M. A. Uman, An improved return stroke model with specified channel-base current, J. Geophys. Res. Atmos. 95 (D9) (1990) 13,621–13,644.

[19] J. M. Cvetić, B. V. Stanić, F. Heidler, Properties of the Channel Discharge Function in the Generalized Lightning Travelling Current Source Return Stroke Model, in: Proc. 13th Int. Zurich Symp. and Technical Exhibition on Electromagnetic Compatibility, Swiss Fed. Inst. of Technol., Zurich, Switzerland, 1999, pp. 575–580.

[20] J. Cvetic, P. Osmokrovic, F. Heidler, Z. Trifkovic, Extension of Lightning Corona Sheath Model during Return Stroke, IEEE Trans. Dielectr. Electr. Insul. 18 (5) (2011) 1383–1392.

[21] V. Cooray, N. Theethayi, Pulse Propagation Along Transmission Lines in the Presence of Corona and Their Implication to Lightning Return Strokes, IEEE Trans. Antennas Propag. 56 (7) (2008) 1948–1959.

[22] V. Cooray, A Novel Procedure to Represent Lightning Return Strokes – Current Dissipation Return Stroke Models, IEEE Trans. Electromagn. Compat. 51 (3) (2009) 748–755.

[23] J. S. Boyle, R. E. Orville, Return stroke velocity measurements in multistroke lightning flashes, J. Geophys. Res. Atmos. 81 (24) (1976) 4461–4466.

[24] K. Berger, Parameters of lightning flashes, Electra 41 (1975) 23–37.

[25] G. Diendorfer, H. Pichler, M. Mair, Some parameters of negative upward-initiated lightning to the Gaisberg tower (2000–2007), IEEE Trans. Electromagn. Compat. 51 (3) (2009) 443–452.

[26] A. M. Hussein, W. Janischewskyj, M. Milewski, V. Shostak, W. Chisholm, J. S. Chang, Current waveform parameters of CN tower lightning return strokes, J. Electrostat. 60 (2-4) (2004) 149–162.

[27] C. Romero, A. Rubinstein, M. Paolone, F. Rachidi, M. Rubinstein, P. Zweiacker, B. Daout, Instrumentation of the Säntis Tower in Switzerland for Lightning Current Measurements, Int. J. Plasma Environ. Sci. Technol. 4 (1) (2010) 86–92.

[28] C. Romero, F. Rachidi, M. Rubinstein, M. Paolone, Lightning Currents Measured on the Säntis Tower: A Summary of the Results Obtained in 2010 and 2011, in: 2013 IEEE International Symposium on Electromagnetic Compatibility, Denver, Colorado, 2013, pp. 825–828.

[29] F. Heidler, Analytische blitzstromfunktion zur LEMP-berechnung, in: Proc. 18th Int. Conf. Lightning Protection, Munich, Germany, 1985, pp. 63–66 (paper 1.9).

[30] F. Heidler, J. M. Cvetić, B. V. Stanić, Calculation of Lightning Current Parameters, IEEE Trans. Power Del. 14 (2) (1999) 399–404.

[31] F. Heidler, J. M. Cvetić, A class of analytical functions to study the lightning effects associated with the current front, Eur. Trans. Electr. Power 12 (2) (2002) 141–150.

[32] A. Andreotti, A. Pierno, L. Verolino, A New Channel-Base Current Model for Lightning-Induced Voltage Calculations, IEEE Trans. Electromagn. Compat. 61 (3) (2019) 617–622.

[33] V. Javor and P. D. Rancic, A Channel-Base Current Function for Lightning Return-Stroke Modeling, IEEE Trans. Electromagn. Compat. 53 (1) (2011) 245–249.

[34] D. Mestriner, M. Brignone, R. Procopio, A. Piantini, F. Rachidi, A New Channel-Base Lightning Current Formula With Analytically Adjustable Parameters, IEEE Trans. Electromagn. Compat. 63 (2) (2021) 542–549.

[35] V. Cooray, M. Rubinstein, F. Rachidi, Modified Transmission Line Model with a Current Attenuation Function Derived from the Lightning Radiation Field - MTLD Model, Atmosphere 12 (249) (2021) 1–24.

[36] A. Andreotti, U. De Martinis, and L. Verolino, An Inverse Procedure for the Return Stroke Current Identification, IEEE Trans. Electromagn. Compat. 43 (2) (2001) 155–160.

[37] F. Delfino, R. Procopio, A. Andreotti, L. Verolino, Lightning return stroke current identification via field measurement, Electr. Eng. 84 (2002) 41–50.

[38] A. Andreotti, D. Assante, S. Falco, L. Verolino, An Improved Procedure for the Return Stroke Current Identification, IEEE Trans. Magn. 41 (5) (2005) 1872–1875.

[39] A. Ceclan, V. Ţopa, D. D. Micu, A. Andreotti, Lightning-Inverse Reconstruction by Remote Sensing and Numerical-Field Synthesis, IEEE Trans. Magn. 49 (5) (2013) 1657–1660.

[40] M. Brignone, D. Mestriner, R. Procopio, F. Delfino, A review on the return stroke engineering models attenuation function: Proposed expressions, validation and identification methods, Electr. Pow. Syst. Res. 172 (2019) 230–241.

[41] R. Aramini, M. Brignone, D. Mestriner, M. Pastorino, R. Procopio, A. Randazzo, M. Rubinstein, On the Fourier Transform of Measured Electric Fields Radiated by a Lightning Return Stroke, IEEE Trans. Electromagn. Compat. (in press) (2022).

[42] F. Rachidi, C. A. Nucci, M. Ianoz, C. Mazzetti, Influence of a Lossy Ground on Lightning-Induced Voltages on Overhead Lines, IEEE Trans.

Electromag. Compat. 38 (3) (1996; with errata corrige, ibid., vol. 39, no. 2, p. 187, 1997) 250–264.

[43] M. A. Uman, D. K. McLain, E. P. Krider, The Electromagnetic Radiation from a Finite Antenna, Am. J. Phys. 43 (1975) 33–38.

[44] V. Cooray, An Introduction to Lightning, Springer, Dordrecht, 2015, pp. 167–185.

[45] F. Rachidi, W. Janischewskyj, A. M. Hussein, C. A. Nucci, S. Guerrieri, B. Kordi, J.-S. Chang, Current and Electromagnetic Field Associated With Lightning–Return Strokes to Tall Towers, IEEE Trans. Electromag. Compat. 43 (3) (2001) 356–367.

[46] D. Colton, R. Kress, Inverse Acoustic and Electromagnetic Scattering Theory, 4th Edition, Springer, Berlin, 2019, pp. 179–180.

[47] J. C. Willett, J. C. Bailey, V. P. Idone, A. Eybert-Berard, L. Barret, Submicrosecond Intercomparison of Radiation Fields and Currents in Triggered Lightning Return Strokes Based on the Transmission-Line Model, J. Geophys. Res. 94 (D11) (1989) 13,275–13,286.

[48] M. Bertero, P. Boccacci, Introduction to Inverse Problems in Imaging, Institute of Physics Publishing, Bristol, 1998, pp. 39–40.

[49] CIGRE Working Group C4.407, Lightning Parameters for Engineering Applications, CIGRE Publication (2013) 1–117.

[50] H. W. Engl, M. Hanke, A. Neubauer, Regularization of Inverse Problems, Kluwer Academic Publishers, Dordrecht, 1996.

[51] P. C. Hansen, Analysis of discrete ill-posed problems by means of the L-curve, SIAM Rev. 34 (4) (1992) 561–580.

[52] P. C. Hansen, Regularization Tools, a MATLAB Package for Analysis and Solution of Discrete Ill-Posed Problems (2008).
URL {http://www.imm.dtu.dk/~pcha/Regutools/RTv4manual.pdf}